Paired Electrosynthesis of H_2 and Acetic Acid at A/cm^2 Current Densities

Cong Tian,[‡] Xiao-Yan Li,[‡] Vivian E. Nelson,[‡] Pengfei Ou, Daojin Zhou, Yuanjun Chen, Jinqiang Zhang, Jianan Erick Huang, Ning Wang, Jiaqi Yu, Hengzhou Liu, Cheng Liu, Yi Yang, Tao Peng, Yong Zhao, Byoung-Hoon Lee, Sasa Wang, Erfan Shirzadi, Zhu Chen, Rui Kai Miao, David Sinton,* and Edward H. Sargent*

ACCESS | Metrics & More | Article Recommendations | SI Supporting Information

ABSTRACT: Industrial water splitting pairs cathodic hydrogen evolution with oxygen evolution at the anode, the latter generating low-value oxygen as the oxidative product. We reasoned that replacing the oxygen evolution reaction (OER) with anodic electrosynthesis of acetic acid from ethanol at industrial current densities could be a route to increase the economic efficiency of green hydrogen production. We partition the selective oxidation of ethanol to acetic acid into two mechanistically distinct transformations: first ethanol oxidation followed by the production of *OH. Density functional theory (DFT) studies show that the aldehyde-derived intermediate CH_3CO* from ethanol oxidation and the *OH radical from water dissociation are both needed in the electroproduction of acetic acid. *Operando* Fourier transform infrared (FTIR) spectroscopy identifies the corresponding aldehyde intermediates on the anode surface. Based on these mechanistic findings, we develop a vacancy-rich $IrRuO_x$ catalyst and achieve selective electrotransformation of ethanol to acetic acid at a generation rate of 30 mmol/cm^2/h and a partial current density of 3 A/cm^2, fully 10× higher than in the previous highest-activity reports.
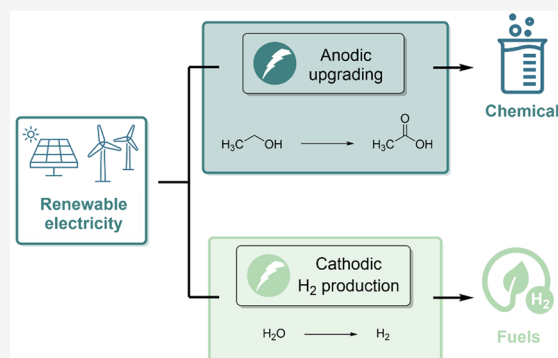
Hydrogen (H_2) electroproduction is typically accompanied by the production of oxygen at the anode. The more limited economic value of the oxygen (O_2) emerging from the oxygen evolution reaction (OER) suggests opportunities to seek alternative anodic products that might help to widen the adoption of low-carbon-intensity hydrogen.[1]

Alternative anodic reactions[2−6] that generate higher-value anodic products are thus of interest (Figure 1A). To date, though, the productivity of these approaches has remained below the ∼A/cm^2 level required for application (Figure 1B).

Ethanol, a biomass feedstock with an annual production rate of more than 77 million metric tons,[7] has been researched in depth in direct ethanol fuel cells (DEFCs) as a high energy density material, in which 12 electron transfers occur per mole of ethanol and CO_2 is formed as the chemical product.[8−11] We aim here instead at valorizing ethanol, targeting its selective electrooxidation, and minimizing undesired CO_2 production.

We investigate ethanol oxidation toward the commodity chemical acetic acid. At 15 million metric tons per year,[12] acetic acid is used to produce paints, adhesives, solvents, and plastics. Currently, acetic acid is manufactured via the Monsanto process,[13] a homogeneous rhodium-catalyzed methanol carbonylation route which operates at high temper-atures (150−200 °C) and pressures (3−10 MPa) (Figure S1) and generates 1 ton of CO_2 emissions per ton of acetic acid.[12]

Electrocatalytic approaches have been pursued in the production of acetic acid (Figure 1C), including via ethanol electrooxidation[8,14,15] (Table S2), carbon dioxide reduction (CO_2R),[16−18] and carbon monoxide reduction (COR)[19−23] (Figure 1C). Most recently, pairing H_2 production and alcohol oxidation[14,24,25] has been advanced as a valorization strategy. The anodic products improve electron utilization in a paired system and benefit overall atomic economy in green H_2 production (Figure 1C and Table S6).

To date, though, these approaches have been limited to alkaline media, resulting in acetate salts that require an additional protonation step to produce acetic acid. In general, prior reports of the anodic oxidation of ethanol were operated
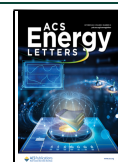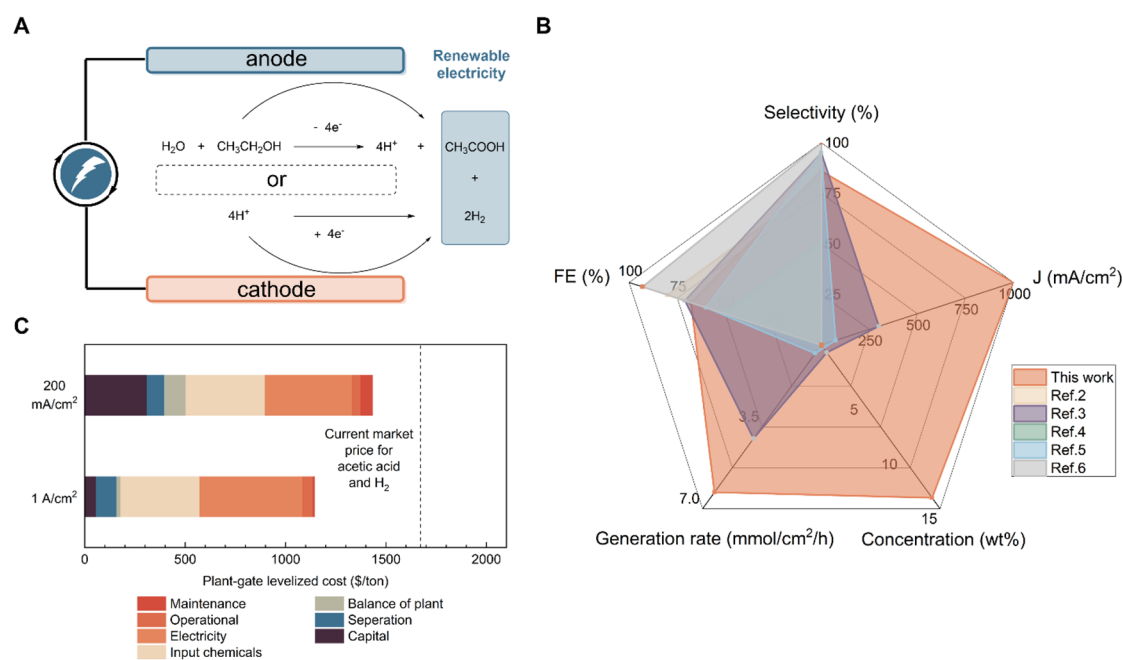
Figure 1. Anodic oxidation of ethanol to acetic acid. (A) Schematic showing coupled electrochemical H_2 and acetic acid production. (B) Comparison of product concentration, faradaic efficiency, generation rate, stability, and current density for state-of-the-art alternative anodic reactions.[2−6] (C) Technoeconomic analysis (TEA) for electrosynthesis of acetic acid using anodic oxidation of ethanol in an acidic electrolyte. The input chemicals and electricity cost make up the major cost in the plant-gate-levelized cost for the paired system. The current market price represents the sum of the values of the market prices of 1 ton of acetic acid plus the H_2 cogenerated per 1 ton of acetic acid.
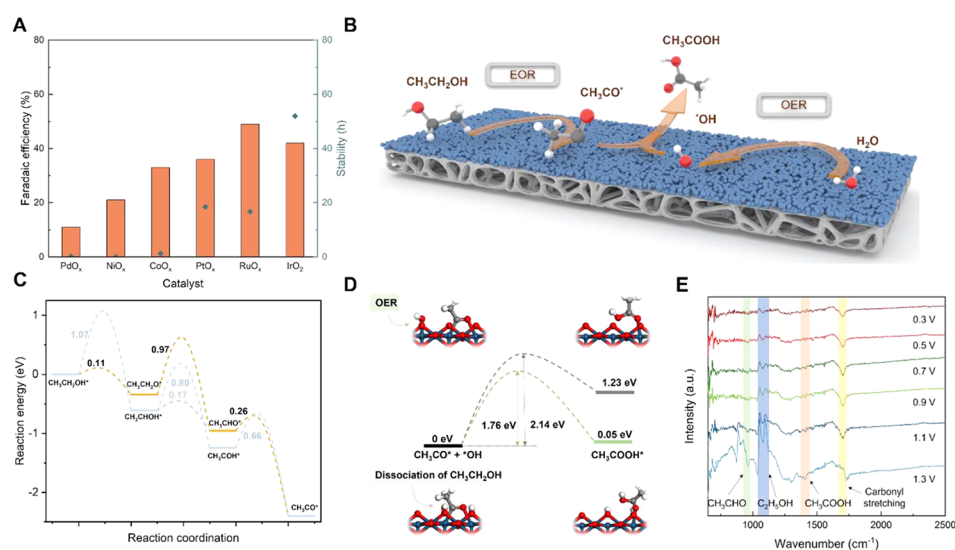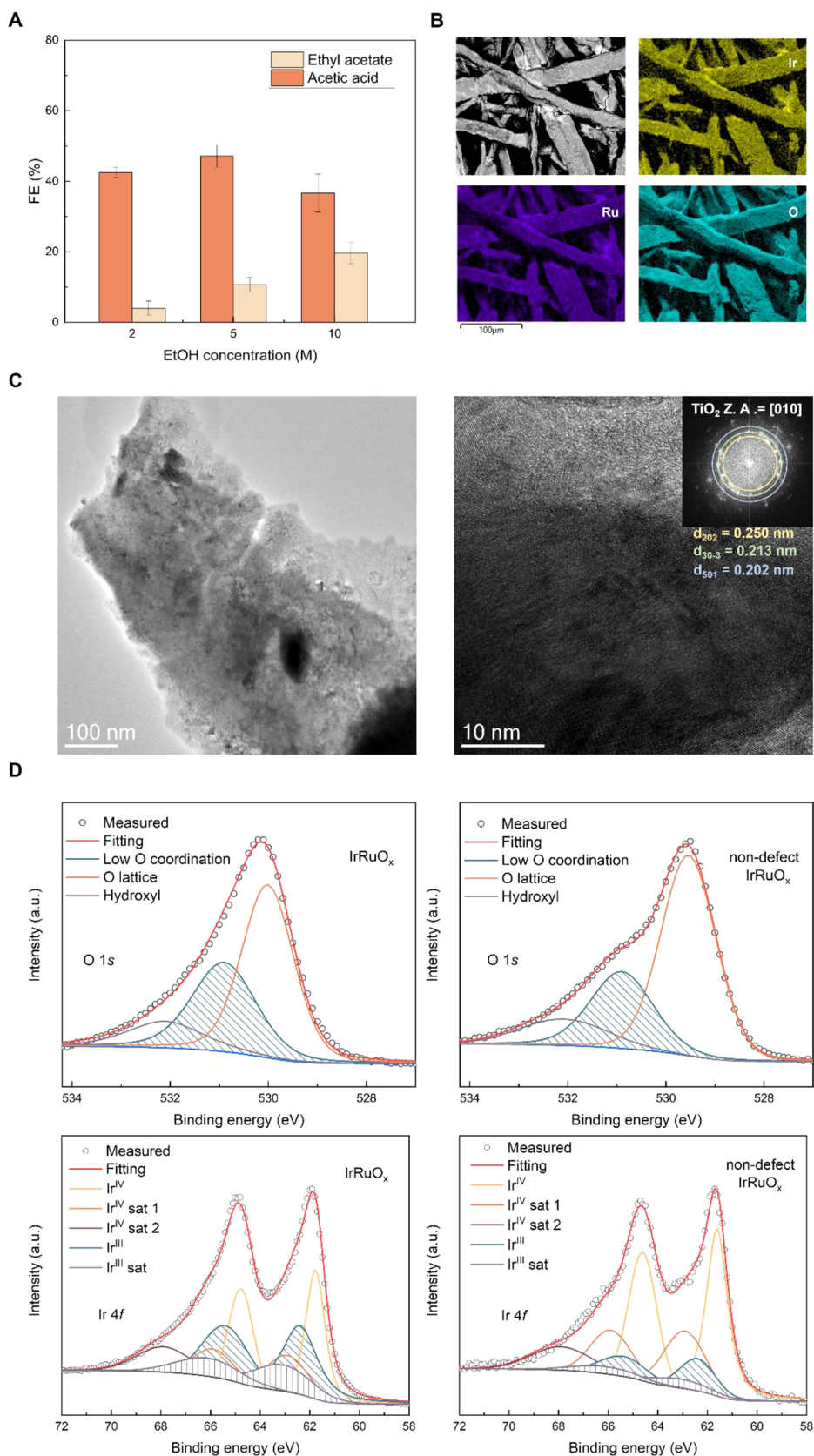

Figure 2. Proposed mechanism of electrocatalytic acetic acid production. (A) Catalyst screening for ethanol oxidation. (B) Schematic of the proposed mechanism for high-rate acetic acid production on the anode. (C) DFT calculation for possible reaction pathways in ethanol oxidation to CH_3CO^*. (D) Comparison of energy barriers for coupling of $^*OH$ from the OER and ethanol dissociation. (E) *Operando* IR spectroscopy for acetic acid production on the IrO_2 catalyst under different potentials versus Ag/AgCl in 5 M EtOH and 1 M H_2SO_4 electrolyte.

in alkaline media and exhibited low current densities (<200 mA/cm²).[14]

We focused instead on seeking an anodic valorization of ethanol that would couple readily to acidic PEM water electrolysis. A technoeconomic analysis (Figure 1D and Table S4) indicates the importance of striving for higher current densities.

We initiated our studies by screening catalysts (Figure 2A) in an approach that, to avoid the energy-intensive acetate protonation step, employed 1 M sulfuric acid (H_2SO_4) as the electrolyte. A set of transition metal and transition metal oxide catalysts reported to be active in alcohol oxidation[10,8,25−27] were loaded on titanium (Ti) felt and used as the anode. Acetic acid was detected in the anolyte using ^1H nuclear magnetic resonance (NMR) spectroscopy (Figure S2).

Figure 3. Electrochemical performance. (A) Electroproduction of acetic acid and ethyl acetate with different ethanol concentrations. (B) EDS and (C) TEM images reveal the distribution of Ir, Ru, and O on the IrRuO$_x$/Ti felt catalyst. (D) XPS fitting of Ir 4f and O 1s shows the surface vacancies of the IrRuO$_x$ catalyst.

Transition metal catalysts with demonstrated activity for alcohol oxidation at low current densities (<50 mA/cm^2), such as cobalt oxide, nickel oxide, palladium oxide, and platinum oxide, were tested at 200 mA/cm^2 but lacked both faradaic efficiency and stability (Figure S3 and Table S3).

We observed encouraging acetic acid generation and good durability using iridium oxide and ruthenium oxide anodes with 42% and 49% FE, respectively, at 200 mA/cm^2. In particular, the IrO$_2$ catalyst produced acetic acid continuously for more than 50 h.

We investigated the catalytic mechanism, building on previous studies[28] that suggested the coupling of surface-absorbed aldehydes and hydroxides is a key step in delivering carboxylic acids. However, we observed the limited presence of the required hydroxide, something we attributed to operating at high current densities in an acidic electrolyte.[29] We sought approaches that would catalyze, sequentially, these two steps (Figure 2B): alcohol oxidation to generate aldehyde and water-splitting to form hydroxide.[30] This, we posited, would ensure the selective ethanol oxidation to acetic acid and would suppress the OER simultaneously. We focused on a study of IrO$_2$ to test these ideas.

Using density functional theory (DFT), we studied the reaction mechanism on the O-terminated surface of IrO$_2$(110) (Figures S9−S11). The overall reaction pathway can be divided into two stages: an ethanol dehydrogenation stage and an *OH coupling stage. In the dehydrogenation stage, the dehydrogenation of ethanol to generate CH$_3$CO* has several possible routes that go through distinct intermediates (Figure 2C). O−H cleavage of the oxygen atom to form CH$_3$CH$_2$O* is the most energetically favored pathway, with an energy barrier of 0.11 eV. Thereafter, the second dehydrogenation intermediate CH$_3$CHO* is obtained by breaking the C−H bond, overcoming an energy barrier of 0.97 eV, which is the rate-determining step in the dehydrogenation process. The acetaldehyde intermediate CH$_3$CHO* is further dehydrogenated into CH$_3$CO* with an energy barrier of 0.20 eV and concludes the first stage. In the second stage, the CH$_3$CO* intermediate reacts with *OH and forms the target product, acetic acid (Figure 2D). We found that the CH$_3$CO* species prefer to couple with *OH radicals generated from the dissociation of water with an energy barrier of 1.78 eV while reacting with the *OH generated from the dehydrogenation of ethanol presents a higher energy barrier of 2.14 eV. The DFT studies agree with the idea that the aldehyde-derived intermediate CH$_3$CO* and the generation of *OH radicals from the dissociation of water together facilitate acetic acid electroproduction.
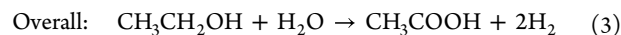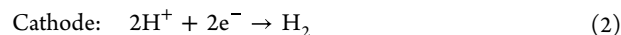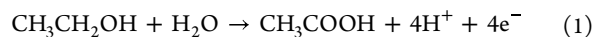
Experimentally, we first introduced the postulated intermediate CH$_3$CHO* by conducting acetaldehyde oxidation on IrO$_2$/Ti. An acetic acid FE of 90% was achieved at an industrial water-splitting current density of 1 A/cm^2 (Figure S4). To check for experimental signals of aldehyde intermediates, we conducted *operando* IR spectroscopy measurements during ethanol oxidation (Figure 2E and Figure S5A). Electrochemical *in situ* IR spectroscopy was performed under positive potentials from 0.3 to 1.3 V versus Ag/AgCl. No band for CO$_2$ formation[8] was detected at 2343 cm^{-1}. The absence of CO$_2$ evolution was further confirmed by gas-phase chromatography, indicating that reactant ethanol is selectively oxidized to the desired acetic acid. The characteristic bands found at 939 cm^{-1} are suggestive of the surface formation of acetaldehyde,[9,31] an intermediate formed from ethanol oxidation, one whose signal

increased notably with increasing potential. This, as noted above, sets the stage for coupling to the generated *OH radicals. We conducted ^{18}O isotope-labeled experiments using H$_2{}^{18}$O to ascertain whether coupling implicated *OH species generated from the dissociation of water. We found evidence of CH$_3$CO^{18}OH in direct analysis real-time mass spectrometry (DART-MS) (Figure S5B), in agreement with the mechanistic picture presented above.
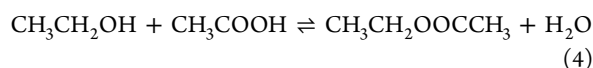
We conducted electrooxidation of ethanol at 1 A/cm^2 using different ethanol concentrations, and rather than observing a dependence on applied current or reaction potential, we found instead that ethyl acetate production increased with ethanol concentration (Figure 3A); this finding is consistent with the idea that ethyl acetate is formed by facile esterification between ethanol and the anodic oxidation product acetic acid (eqs 1−4).

Ethyl acetate formation can be reduced by lowering the ethanol concentration or by removing the acetic acid from the electrolyte. The ethyl acetate formed can serve as an azeotroping agent[13] in the separation of acetic acid from the aqueous phase:

Anode:

$$CH_3CH_2OH + H_2O \rightarrow CH_3COOH + 4H^+ + 4e^- \quad (1)$$

Cathode: $\quad 2H^+ + 2e^- \rightarrow H_2 \quad (2)$

Overall: $\quad CH_3CH_2OH + H_2O \rightarrow CH_3COOH + 2H_2 \quad (3)$

Esterification:

$$CH_3CH_2OH + CH_3COOH \rightleftharpoons CH_3CH_2OOCCH_3 + H_2O \quad (4)$$

Even at the optimal EtOH concentration, the electrochemical performance of IrO$_2$ displays low acetic acid FE and high full cell potential that hinder its economic feasibility (Figure S6).

Based on the above mechanistic findings, we turned to improved working electrode designs. With the goal of further increasing surface-generated aldehyde and hydroxy species, we developed a vacancy-rich[32] IrRuO$_x$ on Ti felt anode, a catalyst formed with the aid of Zn doping and ensuing chemical etching.[33] We looked at the catalyst structure, finding with TEM (Figure 3C) that IrRuO$_x$ nanoparticles were homogeneously dispersed on the Ti felt after the thermal decomposition process.[34] A uniform distribution of Ir, Ru, and O on the Ti support is seen in energy dispersive spectroscopy (EDS) (Figure 3B). To investigate whether vacancies were generated after chemical etching, we prepared a control catalyst, IrRuO$_x$, using a method the same in all respects except that we added no Zn and did not complete any further etching. X-ray photoelectron spectroscopy (XPS) characterization (Figure 3D and Figure S7) was applied to IrO$_2$, IrRuO$_x$, and nondefect IrRuO$_x$. Deconvolution of O 1s XPS profiles shows peaks for lattice oxygen, surface hydroxyl, and defect sites with a low oxygen coordination at 530.1, 532.2, and 530.9 eV, respectively.[32,35,36] The low oxygen coordination peak area in IrRuO$_x$ is 34.7%, which is higher than that of nondefective IrRuO$_x$ (27.6%), indicating an increase in oxygen vacancy.[32] The deconvolved peaks of Ir 4f spectra with Ir^{III} and Ir^{IV} states are also shown in Figure 3D. The defective IrRuO$_x$ has the higher Ir^{III}, species compared with nondefective IrRuO$_x$, which is consistent with the generation of more vacancies on the defective RuIrO$_x$.[37,38] Linear sweep voltammetry (LSV) (Figure 4A) revealed that the potential
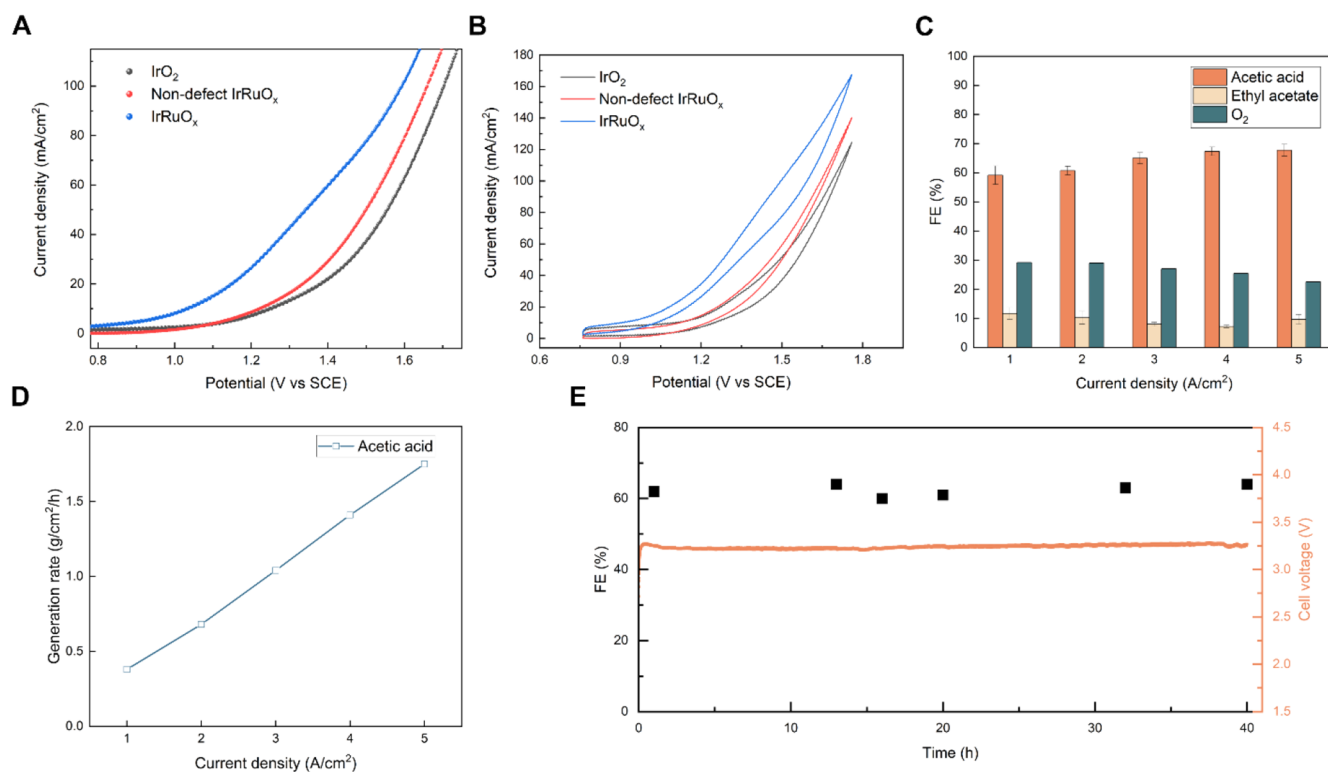
Figure 4. Evaluation of acetic acid production. (A) Linear sweep voltammetry spectra and (B) cyclic voltammetry spectra recorded at 50 mV/s in 0.5 M H_2SO_4 and 5 M EtOH without *iR* correction. (C) Acetic acid production at ampere-level current densities. (D) Electroproduction of acetic acid generation rate at different current densities. (E) Acetate FE and cell voltage during 40 h of acetic acid production at 1 A/cm^2 using the IrRuO$_x$/Ti catalyst.

of IrRuO$_x$ at 20 mA/cm^2 was ∼230 mV lower than IrO$_2$ and ∼180 mV lower than nondefective IrRuO$_x$. Cyclic voltammetry (CV) experiments (Figure 4B) showed a broad oxidation curve of acetic acid at around 1.5 V versus SCE in 0.5 M H_2SO_4 and 5 M ethanol solution.

We then explored strategies to operate the acetic acid production at high current densities that can be readily coupled with an industrial hydrogen generation reaction (Figure 4C). We achieved 5 A/cm^2 anodic acetic acid synthesis, a 13× higher generation rate than in the prior highest-productivity reports.[23] At 1 A/cm^2 over 12 h, we obtained a 14 wt % concentration of acetic acid (Figure S8). At 5 A/cm^2 (Table S5) and using 1 cm^2 electrolyzer surface area, we achieved gram-scale (1.75 g/cm^2/h) electrosynthesis of acetic acid in under 1 h (Figure 4D).

Gas-phase chromatography indicates that the remaining charge can be accounted for via the conversion of the OER to O_2. No other oxidation products were found. No CO_2 was detected within the limits of detection in gas-phase analysis, in agreement with our *in situ* IR finding that ethanol oxidation is selective toward acetic acid production.

We probed the stability of the IrRuO$_x$/Ti anode during the oxidative production of acetic acid at 1 A/cm^2. It maintained an average acetate (acetic acid and ethyl acetate) FE of 62% over the course of 40 h of continuous electrosynthesis in the MEA (Figure 4E) at no more than 3.25 V full cell potential, which is decreased by over 450 mV compared to the IrO$_2$/Ti anode. A portion of the electrolyte was periodically removed to analyze the composition and replaced with fresh electrolyte during the stability test.

This work reports the electrosynthesis of acetic acid at current densities of interest in H_2 coproduction. Instead of suppressing the O_2 evolution side reaction, this approach relies on both ethanol oxidation and water splitting from the OER. An acetic acid FE of 59−68% along with 8−11% FE toward ethyl acetate at ampere-level current densities was achieved using this strategy. With mechanistic insights provided by DFT and in situ spectroscopies, a direct anodic upgrading strategy at record production rates was developed. This method of acetic acid electrosynthesis operates continuously with a full cell voltage of less than 3.25 V at 1 A/cm^2 with an average acetate FE of 62%. This work provides a strategy for designing other electrooxidation reactions with a high current efficiency and indicates a route to decarbonization in the H_2 production industry. Further advances can be achieved through new catalyst and system design to achieve increased energy efficiency, as well as the search for durable, cost-effective, and PGM-free metal catalysts. Additionally, coelectrolysis[39,40] of CO_2 reduction at the cathode and ethanol oxidation at the anode produces acetic acid on both sides of the electrolyzer and holds potential to further increase the energy efficiency and carbon utilization in electrochemical acetic acid production.

■ ASSOCIATED CONTENT

ⓢ Supporting Information

The Supporting Information is available free of charge at https://pubs.acs.org/doi/10.1021/acsenergylett.3c01327.

Materials and methods, catalyst preparation, catalyst characterization, TEA calculation, comparison with

literature results, product analysis, faradaic efficiencies, FTIR spectroscopies, XPS, and DFT calculations (PDF)

AUTHOR INFORMATION

Corresponding Authors

David Sinton − *Department of Mechanical and Industrial Engineering, University of Toronto, Toronto, Ontario M5S 3G8, Canada;* orcid.org/0000-0003-2714-6408; Email: sinton@mie.utoronto.ca

Edward H. Sargent − *Department of Electrical and Computer Engineering, University of Toronto, Toronto, Ontario M5S 3G4, Canada; Department of Chemistry and Department of Electrical and Computer Engineering, Northwestern University, Evanston, Illinois 60208, United States;* orcid.org/0000-0003-0396-6495; Email: ted.sargent@utoronto.ca

Authors

Cong Tian − *Department of Electrical and Computer Engineering, University of Toronto, Toronto, Ontario M5S 3G4, Canada; Department of Chemistry, Northwestern University, Evanston, Illinois 60208, United States;* orcid.org/0000-0002-1260-3402

Xiao-Yan Li − *Department of Electrical and Computer Engineering, University of Toronto, Toronto, Ontario M5S 3G4, Canada; Department of Chemistry, Northwestern University, Evanston, Illinois 60208, United States;* orcid.org/0009-0003-2325-7538

Vivian E. Nelson − *Department of Mechanical and Industrial Engineering, University of Toronto, Toronto, Ontario M5S 3G8, Canada*

Pengfei Ou − *Department of Electrical and Computer Engineering, University of Toronto, Toronto, Ontario M5S 3G4, Canada; Department of Chemistry, Northwestern University, Evanston, Illinois 60208, United States*

Daojin Zhou − *Department of Electrical and Computer Engineering, University of Toronto, Toronto, Ontario M5S 3G4, Canada; Department of Chemistry, Northwestern University, Evanston, Illinois 60208, United States*

Yuanjun Chen − *Department of Electrical and Computer Engineering, University of Toronto, Toronto, Ontario M5S 3G4, Canada; Department of Chemistry, Northwestern University, Evanston, Illinois 60208, United States*

Jinqiang Zhang − *Department of Electrical and Computer Engineering, University of Toronto, Toronto, Ontario M5S 3G4, Canada;* orcid.org/0000-0001-5476-0134

Jianan Erick Huang − *Department of Electrical and Computer Engineering, University of Toronto, Toronto, Ontario M5S 3G4, Canada*

Ning Wang − *Department of Electrical and Computer Engineering, University of Toronto, Toronto, Ontario M5S 3G4, Canada;* orcid.org/0000-0002-2589-6881

Jiaqi Yu − *Department of Chemistry, Northwestern University, Evanston, Illinois 60208, United States*

Hengzhou Liu − *Department of Chemistry, Northwestern University, Evanston, Illinois 60208, United States*

Cheng Liu − *Department of Chemistry, Northwestern University, Evanston, Illinois 60208, United States*

Yi Yang − *Department of Chemistry, Northwestern University, Evanston, Illinois 60208, United States;* orcid.org/0000-0002-7775-6856

Tao Peng − *Department of Electrical and Computer Engineering, University of Toronto, Toronto, Ontario M5S 3G4, Canada;* orcid.org/0000-0001-8517-5368

Yong Zhao − *Department of Mechanical and Industrial Engineering, University of Toronto, Toronto, Ontario M5S 3G8, Canada*

Byoung-Hoon Lee − *Department of Electrical and Computer Engineering, University of Toronto, Toronto, Ontario M5S 3G4, Canada*

Sasa Wang − *Department of Electrical and Computer Engineering, University of Toronto, Toronto, Ontario M5S 3G4, Canada*

Erfan Shirzadi − *Department of Electrical and Computer Engineering, University of Toronto, Toronto, Ontario M5S 3G4, Canada*

Zhu Chen − *Department of Electrical and Computer Engineering, University of Toronto, Toronto, Ontario M5S 3G4, Canada*

Rui Kai Miao − *Department of Mechanical and Industrial Engineering, University of Toronto, Toronto, Ontario M5S 3G8, Canada*

Complete contact information is available at:
https://pubs.acs.org/10.1021/acsenergylett.3c01327

Author Contributions

[‡]C.T., X.-Y.L., and V.E.N. contributed equally.

Notes

The authors declare no competing financial interest.

REFERENCES

(1) Suen, N.-T.; Hung, S.-F.; Quan, Q.; Zhang, N.; Xu, Y.-J.; Chen, H. M. Electrocatalysis for the oxygen evolution reaction: Recent development and future perspectives. *Chem. Soc. Rev.* 2017, 46, 337−365.

(2) Lum, Y.; Huang, J. E.; Wang, Z.; Luo, M.; Nam, D.-H.; Leow, W. R.; Chen, B.; Wicks, J.; Li, Y. C.; Wang, Y.; Dinh, C.-T.; Li, J.; Zhuang, T.-T.; Li, F.; Sham, T.-K.; Sinton, D.; Sargent, E. H. Tuning OH binding energy enables selective electrochemical oxidation of ethylene to ethylene glycol. *Nat. Catal.* 2020, 3, 14−22.

(3) Leow, W. R.; Lum, Y.; Ozden, A.; Wang, Y.; Nam, D.-H.; Chen, B.; Wicks, J.; Zhuang, T.-T.; Li, F.; Sinton, D.; Sargent, E. H. Chloride-mediated selective electrosynthesis of ethylene and propylene oxides at high current density. *Science* 2020, 368, 1228−1233.

(4) Liu, D.; Liu, J.-C.; Cai, W.; Ma, J.; Yang, H. B.; Xiao, H.; Li, J.; Xiong, Y.; Huang, Y.; Liu, B. Selective photoelectrochemical oxidation of glycerol to high value-added dihydroxyacetone. *Nat. Commun.* **2019**, *10*, 1779.

(5) Sherbo, R. S.; Delima, R. S.; Chiykowski, V. A.; MacLeod, B. P.; Berlinguette, C. P. Complete electron economy by pairing electrolysis with hydrogenation. *Nat. Catal.* **2018**, *1*, 501−507.

(6) Cha, H. G.; Choi, K.-S. Combined biomass valorization and hydrogen production in a photoelectrochemical cell. *Nat. Chem.* **2015**, *7*, 328−333.

(7) Mika, L. T.; Cséfalvay, E.; Németh, Á. Catalytic conversion of carbohydrates to initial platform chemicals: Chemistry and sustainability. *Chem. Rev.* **2018**, *118*, 505−613.

(8) Wang, Y.; Zheng, M.; Li, Y.; Ye, C.; Chen, J.; Ye, J.; Zhang, Q.; Li, J.; Zhou, Z.; Fu, X. Z.; Wang, J.; Sun, S. G.; Wang, D. p-d Orbital hybridization induced by a monodispersed Ga site on a Pt_3Mn nanocatalyst boosts ethanol electrooxidation. *Angew. Chem., Int. Ed.* **2022**, *61*, No. e202115735.

(9) Liang, Z.; Song, L.; Deng, S.; Zhu, Y.; Stavitski, E.; Adzic, R. R.; Chen, J.; Wang, J. X. Direct 12-electron oxidation of ethanol on a ternary Au(core)-PtIr(shell) electrocatalyst. *J. Am. Chem. Soc.* **2019**, *141*, 9629−9636.

(10) Wang, Y.; Zou, S.; Cai, W.-B. Recent advances on electro-oxidation of ethanol on Pt- and Pd-based catalysts: From reaction mechanisms to catalytic materials. *Catalysts* **2015**, *5*, 1507−1534.

(11) Kowal, A.; Li, M.; Shao, M.; Sasaki, K.; Vukmirovic, M. B.; Zhang, J.; Marinkovic, N. S.; Liu, P.; Frenkel, A. I.; Adzic, R. R. Ternary $Pt/Rh/SnO_2$ electrocatalysts for oxidizing ethanol to CO_2. *Nat. Mater.* **2009**, *8*, 325−330.

(12) Budsberg, E.; Morales-Vera, R.; Crawford, J. T.; Bura, R.; Gustafson, R. Production routes to bio-acetic acid: Life cycle assessment. *Biotechnol. Biofuels* **2020**, *13*, 154.

(13) Le Berre, C.; Serp, P.; Kalck, P.; Torrence, G. P. Acetic acid. In *Ullmann's encyclopedia of industrial chemistry*; Wiley, 2014; pp 1−34.

(14) Zhou, C.-A.; Wang, S.; Ma, K.; Song, L.; Zheng, L.; Yue, H. Membrane-free pure H_2 production over single dispersed Ru-anchored Pt_3Ni alloys via coupling ethanol selective electrooxidation. *Appl. Catal., B* **2023**, *321*, 122065.

(15) Lidasan, J. J. B.; Iguchi, S.; Yamanaka, I. Pure hydrogen production by aqueous ethanol electrolysis on Pt−Ru−O anodes in a solid polymer electrolyte electrolysis cell. *ACS Sustain. Chem. Eng.* **2022**, *10*, 2921−2929.

(16) De, R.; Gonglach, S.; Paul, S.; Haas, M.; Sreejith, S. S.; Gerschel, P.; Apfel, U.-P.; Vuong, T. H.; Rabeah, J.; Roy, S.; Schöfberger, W. Electrocatalytic reduction of CO_2 to acetic acid by a molecular manganese corrole complex. *Angew. Chem., Int. Ed.* **2020**, *59*, 10527−10534.

(17) Zhu, Q.; Sun, X.; Yang, D.; Ma, J.; Kang, X.; Zheng, L.; Zhang, J.; Wu, Z.; Han, B. Carbon dioxide electroreduction to C2 products over copper-cuprous oxide derived from electrosynthesized copper complex. *Nat. Commun.* **2019**, *10*, 3851.

(18) Sun, X.; Zhu, Q.; Kang, X.; Liu, H.; Qian, Q.; Ma, J.; Zhang, Z.; Yang, G.; Han, B. Design of a Cu(I)/C-doped boron nitride electrocatalyst for efficient conversion of CO_2 into acetic acid. *Green Chem.* **2017**, *19*, 2086−2091.

(19) Zhu, P.; Xia, C.; Liu, C.-Y.; Jiang, K.; Gao, G.; Zhang, X.; Xia, Y.; Lei, Y.; Alshareef, H. N.; Senftle, T. P.; Wang, H. Direct and continuous generation of pure acetic acid solutions via electrocatalytic carbon monoxide reduction. *Proc. Natl. Acad. Sci.* **2021**, *118*, No. e2010868118.

(20) Ripatti, D. S.; Veltman, T. R.; Kanan, M. W. Carbon monoxide gas diffusion electrolysis that produces concentrated C2 products with high single-pass conversion. *Joule* **2019**, *3*, 240−256.

(21) Luc, W.; Fu, X.; Shi, J.; Lv, J.-J.; Jouny, M.; Ko, B. H.; Xu, Y.; Tu, Q.; Hu, X.; Wu, J.; Yue, Q.; Liu, Y.; Jiao, F.; Kang, Y. Two-dimensional copper nanosheets for electrochemical reduction of carbon monoxide to acetate. *Nat. Catal.* **2019**, *2*, 423−430.

(22) Jouny, M.; Luc, W.; Jiao, F. High-rate electroreduction of carbon monoxide to multi-carbon products. *Nat. Catal.* **2018**, *1*, 748−755.

(23) Ji, Y.; Chen, Z.; Wei, R.; Yang, C.; Wang, Y.; Xu, J.; Zhang, H.; Guan, A.; Chen, J.; Sham, T.-K.; Luo, J.; Yang, Y.; Xu, X.; Zheng, G. Selective CO-to-acetate electroreduction via intermediate adsorption tuning on ordered Cu−Pd sites. *Nat. Catal.* **2022**, *5*, 251−258.

(24) Li, Z.; Yan, Y.; Xu, S.-M.; Zhou, H.; Xu, M.; Ma, L.; Shao, M.; Kong, X.; Wang, B.; Zheng, L.; Duan, H. Alcohols electrooxidation coupled with H_2 production at high current densities promoted by a cooperative catalyst. *Nat. Commun.* **2022**, *13*, 147.

(25) Liang, Z.; Jiang, D.; Wang, X.; Shakouri, M.; Zhang, T.; Li, Z.; Tang, P.; Llorca, J.; Liu, L.; Yuan, Y.; Heggen, M.; Dunin-Borkowski, R. E.; Morante, J. R.; Cabot, A.; Arbiol, J. Molecular engineering to tune the ligand environment of atomically dispersed nickel for efficient alcohol electrochemical oxidation. *Adv. Funct. Mater.* **2021**, *31*, 2106349.

(26) Zhou, X.; Ma, Y.; Ge, Y.; Zhu, S.; Cui, Y.; Chen, B.; Liao, L.; Yun, Q.; He, Z.; Long, H.; Li, L.; Huang, B.; Luo, Q.; Zhai, L.; Wang, X.; Bai, L.; Wang, G.; Guan, Z.; Chen, Y.; Lee, C.-S.; Wang, J.; Ling, C.; Shao, M.; Fan, Z.; Zhang, H. Preparation of Au@Pd core−shell nanorods with fcc-2h-fcc heterophase for highly efficient electro-catalytic alcohol oxidation. *J. Am. Chem. Soc.* **2022**, *144*, 547−555.

(27) Dai, L.; Qin, Q.; Zhao, X.; Xu, C.; Hu, C.; Mo, S.; Wang, Y. O.; Lin, S.; Tang, Z.; Zheng, N. Electrochemical partial reforming of ethanol into ethyl acetate using ultrathin Co_3O_4 nanosheets as a highly selective anode catalyst. *ACS Cent. Sci.* **2016**, *2*, 538−544.

(28) Kwon, Y.; Lai, S. C. S.; Rodriguez, P.; Koper, M. T. M. Electrocatalytic oxidation of alcohols on gold in alkaline media: Base or gold catalysis? *J. Am. Chem. Soc.* **2011**, *133*, 6914−6917.

(29) Li, L.; Wang, P.; Shao, Q.; Huang, X. Recent progress in advanced electrocatalyst design for acidic oxygen evolution reaction. *Adv. Mater.* **2021**, *33*, 2004243.

(30) Camp, J. E. Auto-tandem catalysis: Activation of multiple, mechanistically distinct process by a single catalyst. *Eur. J. Org. Chem.* **2017**, *2017*, 425−433.

(31) Raskó, J.; Kecskés, T.; Kiss, J. Ft-ir and mass spectrometric studies on the interaction of acetaldehyde with TiO_2-supported noble metal catalysts. *Appl. Catal. A: Gen.* **2005**, *287*, 244−251.

(32) Ge, R.; Li, L.; Su, J.; Lin, Y.; Tian, Z.; Chen, L. Ultrafine defective RuO_2 electrocatayst integrated on carbon cloth for robust water oxidation in acidic media. *Adv. Energy Mater.* **2019**, *9*, 1901313.

(33) Zhuang, L.; Xu, F.; Wang, K.; Li, J.; Liang, C.; Zhou, W.; Xu, Z.; Shao, Z.; Zhu, Z. Porous structure engineering of iridium oxide nanoclusters on atomic scale for efficient ph-universal overall water splitting. *Small* **2021**, *17*, 2100121.

(34) Luc, W.; Rosen, J.; Jiao, F. An ir-based anode for a practical CO_2 electrolyzer. *Catal. Today* **2017**, *288*, 79−84.

(35) Roginskaya, Y. E.; Morozova, O. V.; Lubnin, E. N.; Ulitina, Y. E.; Lopukhova, G. V.; Trasatti, S. Characterization of bulk and surface composition of $Co_xNi_{1-x}O_y$ mixed oxides for electrocatalysis. *Langmuir* **1997**, *13*, 4621−4627.

(36) Bao, J.; Zhang, X.; Fan, B.; Zhang, J.; Zhou, M.; Yang, W.; Hu, X.; Wang, H.; Pan, B.; Xie, Y. Ultrathin spinel-structured nanosheets rich in oxygen deficiencies for enhanced electrocatalytic water oxidation. *Angew. Chem.* **2015**, *127*, 7507−7512.

(37) Pfeifer, V.; Jones, T. E.; Velasco Vélez, J. J.; Massué, C.; Greiner, M. T.; Arrigo, R.; Teschner, D.; Girgsdies, F.; Scherzer, M.; Allan, J.; Hashagen, M.; Weinberg, G.; Piccinin, S.; Hävecker, M.; Knop-Gericke, A.; Schlögl, R. The electronic structure of iridium oxide electrodes active in water splitting. *Phys. Chem. Chem. Phys.* **2016**, *18*, 2292−2296.

(38) Pfeifer, V.; Jones, T. E.; Velasco Vélez, J. J.; Massué, C.; Arrigo, R.; Teschner, D.; Girgsdies, F.; Scherzer, M.; Greiner, M. T.; Allan, J.; Hashagen, M.; Weinberg, G.; Piccinin, S.; Hävecker, M.; Knop-Gericke, A.; Schlögl, R. The electronic structure of iridium and its oxides. *Surf. Interface Anal.* **2016**, *48*, 261−273.

(39) Verma, S.; Lu, S.; Kenis, P. J. A. Co-electrolysis of CO_2 and glycerol as a pathway to carbon chemicals with improved

technoeconomics due to low electricity consumption. *Nature Energy* **2019**, *4*, 466−474.

(40) Sheng, H.; Janes, A. N.; Ross, R. D.; Hofstetter, H.; Lee, K.; Schmidt, J. R.; Jin, S. Linear paired electrochemical valorization of glycerol enabled by the electro-fenton process using a stable $NiSe_2$ cathode. *Nat. Catal.* **2022**, *5*, 716−725.